Spatially Controlled UV Light Generation at Depth Using Upconversion Micelles

Qi Zhou[1], Brendan M. Wirtz[2], Tracy H. Schloemer[1*], Michael C. Burroughs[2], Manchen Hu[1], Pournima Narayanan[1,3], Junrui Lyu[1], Arynn O. Gallegos[1], Colette Layton[1], Danielle J. Mai[2*], Daniel N. Congreve[1*]

[1]Department of Electrical Engineering, Stanford University, Stanford, CA, USA.

[2]Department of Chemical Engineering, Stanford University, Stanford, CA, USA.

[3]Department of Chemistry, Stanford University, Stanford, CA, USA.

*e-mail: tracyhs@stanford.edu, djmai@stanford.edu, and congreve@stanford.edu

Abstract

Ultraviolet (UV) light can trigger a plethora of useful photochemical reactions for diverse applications, including photocatalysis, photopolymerization, and drug delivery. These applications typically require penetration of high energy photons deep into materials, yet delivering these photons beyond the surface is extremely challenging due to absorption and scattering effects. Triplet-triplet annihilation upconversion (TTA-UC) shows great promise to circumvent this issue by generating high energy photons from incident lower energy photons. However, molecules that facilitate TTA-UC usually have poor water solubility, limiting their deployment in aqueous environments. To address this challenge, we leverage a nanoencapsulation method to fabricate water-compatible UC micelles, enabling on-demand UV photon generation deep into materials. We present two iridium-based complexes for use as TTA-UC sensitizers with increased solubilities that facilitate the formation of highly emissive UV-upconverting micelles. Furthermore, we show this encapsulation method is generalizable to nineteen UV-emitting UC systems, accessing a range of upconverted UV emission profiles with wavelengths as low as 350 nm. As a proof-of-principle demonstration of precision photochemistry at depth, we use UV-emitting UC micelles to photolyze a fluorophore at a focal point nearly a centimeter beyond the surface, revealing opportunities for spatially controlled manipulation deep into UV-responsive materials.

Main

Photochemical processes driven by ultraviolet (UV) light are ubiquitous and span diverse applications such as photocatalysis,[1–3] photopolymerization,[4,5] and biomaterial manipulation for cell culture or drug delivery.[6–8] However, administering UV photons beyond the surface of a material (e.g., deep into a solution or inside biological tissue) is extremely challenging due to high absorption coefficients and scattering losses.[9,10] One strategy to deliver high energy photons at depth is the application of an extremely high light intensity, but this approach wastes energy at the surface and may cause unwanted reactions that further degrade or damage the material.[11–14]

Upconversion (UC), the process of converting low energy photons into higher energy photons, has received significant attention to tackle light penetration issues because visible and infrared photons are generally more transmissive through materials compared to UV photons.[15,16] Using UC, higher energy photons (e.g., UV photons) can be locally generated much deeper into a reaction matrix to activate light-driven reactions using low energy input photons. Among the many reported upconversion pathways and materials,[17–25] triplet-triplet annihilation upconversion (TTA-UC) stands out: high UC efficiencies can be accessed using relatively low input powers, and a wide range of excitation and emission wavelengths have been demonstrated by tuning the system components.[20,26–28] In addition to its potential for high efficiencies and materials tunability, TTA-UC imparts a further benefit inherent in its quadratic nature. Namely, upconversion intensity scales quadratically with input power below a threshold intensity, so precise spatial control of high energy photon generation can be achieved due to efficient upconversion occurring only near the focal point of focused input light. This property has been leveraged to demonstrate TTA-UC-enabled volumetric 3D printing using violet or blue upconverted light.[29–32]

The TTA-UC process is illustrated in **Fig. 1A**. Sensitizers absorb low energy photons, generate triplets *via* spin-orbit coupling, and transfer the triplet states to annihilators through triplet energy transfer. Two annihilator triplet states can then undergo triplet-triplet annihilation to generate one high energy singlet excited state, which can radiatively decay and emit light with more energy than the incident photons. Annihilators for TTA-UC are usually small organic molecules like acenes, whereas sensitizers be a range of materials such as metallic complexes, thermally activated delayed fluorescence (TADF) molecules, and inorganic nanoparticles.[20,27,28]

For UC emission in the UV, a range of sensitizer and annihilator pairs for both blue-to-UV UC[33–43] and green-to-UV UC[44] demonstrate the flexibility of materials options, excitation wavelengths, and emission ranges available to accommodate distinct requirements for different light-driven applications. Yet despite this apparent versatility, sensitizers and annihilators used for UV light generation *via* TTA-UC are usually incompatible with aqueous environments. First, highly polar solvents tend to facilitate electron transfer reactions, which compete with the desired triplet energy transfers between sensitizers and annihilators.[45] Additionally, high local concentrations of materials are required for efficient TTA-UC, but most organic TTA-UC molecules have limited solubility in water. While sensitizers and annihilators can be made water-soluble by appending polar functional groups (i.e., sulfate, carboxylate),[45–47] this approach requires substantial synthetic efforts for each sensitizer and annihilator pair that could result in undesirable changes to their energetic properties and ultimate UC performance.[46]

Here, we employed nanoencapsulation as an alternate method to integrate UC systems into diverse matrices.[29,48–52] After encapsulation, the chemical compatibility of the resultant nanomaterials with a system will dictate the efficiency of delivering upconverted light, thereby overcoming the limitations of individual molecules. We encapsulated UV-emitting UC materials using the block copolymer Pluronic F-127[53–55] to form self-assembled micelles in water. These micelles are comprised of poly(propylene oxide) cores surrounded by poly(ethylene oxide) coronas. UC micelles were fabricated by dissolving UC materials into a high-boiling point organic solvent (1, 2, 4-trichlorobenzene; TCB) that partitions into the hydrophobic core environment of the F-127 micelles.[56–58] The nanoencapsulation method can generalize to different sensitizer and annihilator pairs providing the flexibility of materials choice and UV emission ranges. However, high solubility of the UC materials in TCB are critical to fabricate efficient UV-emitting UC micelles for their subsequent use to perform precise photochemistry at depth.

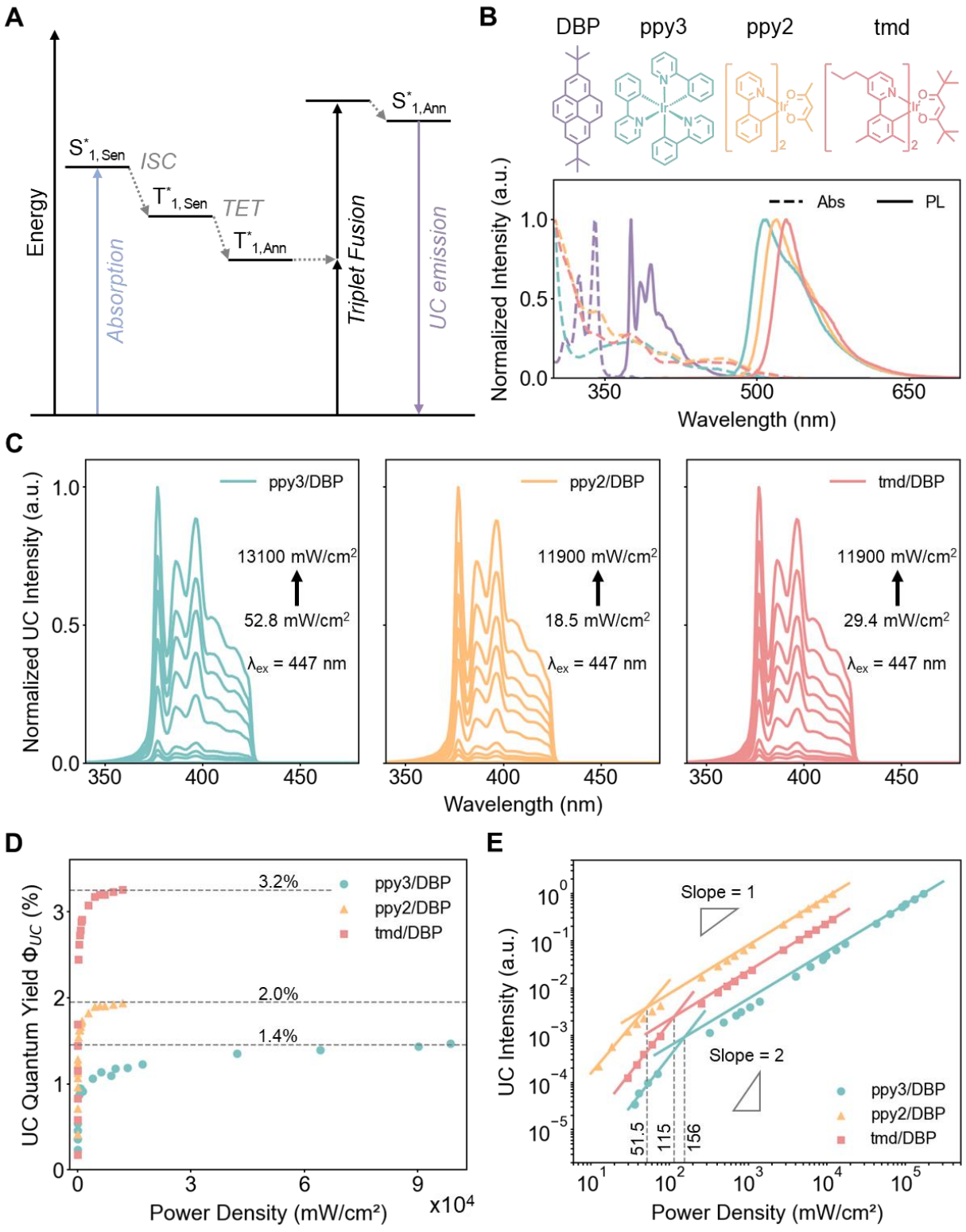

Figure 1. Screening of iridium-based sensitizers reveals versatile TTA-UC pairings with the annihilator DBP in toluene. A. The process of triplet-triplet annihilation upconversion (TTA-

UC): Sensitizers (Sen) absorb lower energy photons and generate triplets *via* intersystem crossing (ISC). Annihilators (Ann) are promoted to their triplet states through triplet energy transfer (TET) from Sen. Two Ann triplets can annihilate to an excited singlet. The Ann singlet emits a higher energy photon, returning to the ground state. **B.** Normalized absorption (Abs) and photoluminescence (PL) spectra of three iridium complexes (ppy3, ppy2, and tmd) and 2,7-di-tert-butylpyrene (DBP). The iridium complexes were excited at 365 nm, and DBP was excited at 335 nm. **C.** Normalized upconversion photoluminescence (UCPL) of sensitizer/annihilator pairs ppy3/DBP, ppy2/DBP, and tmd/DBP in toluene under 447 nm laser excitation with different power densities. UCPL was collected through a 425 nm short pass filter. **D.** UC quantum yields (Φ_{UC}) of ppy3/DBP, ppy2/DBP, and tmd/DBP UC systems in toluene. **E.** UC intensity dependence on incident power for ppy3/DBP, ppy2/DBP, and tmd/DBP UC systems in toluene. The concentrations used for data presented in panels **C**, **D**, and **E** are summarized in **Table S2**.

Inspired by a well-studied blue-to-UV UC sensitizer, tris(2-phenylpyridine)iridium(III), $Ir(ppy)_3$ (ppy3), we identified two promising sensitizers for blue-to-UV UC: bis(2-phenylpyridine)(acetylacetonate)iridium(III), $Ir(ppy)_2(acac)$ (ppy2) and bis(2-(3,5-dimethylphenyl)-4-propylpyridine)(2,2,6,6-tetramethylheptane-3,5-diketonate)iridium(III), $Ir(dmppy\text{-}pro)_2tmd$ (tmd) (**Fig. 1B**). These two iridium complexes are structurally similar to ppy3, but with drastically improved solubilities in the TCB solvent used for micelle fabrication[51] (**Table S1**). During the micelle fabrication process, upconversion molecules are not dispersed evenly across all micelles; rather, upconversion molecules are dispersed following a Poisson distribution.[59] If solubility in TCB is limited, it is difficult to encapsulate enough sensitizers and annihilators within each micelle to enable TTA-UC. For instance, the solubility of ppy3 in both toluene and TCB is less than 1 mM (**Table S1**). Although this solubility is sufficient for UC in bulk solutions (UC materials dissolved in solvents without nanoencapsulation), much higher solubilities are necessary for encapsulation. Modeling the Poisson distribution of ppy3, ppy2, and tmd based on their solubilities in TCB (**Table S1**), average number of molecules per micelle were predicted to be 3, 28, and 74, respectively (**Fig. S1**). This drastic increase in encapsulation efficiency of ppy2 and tmd suggests their potential to improve UC emission in micelles.

Initially, we characterized the UC properties of the iridium complexes ppy2 and tmd with a single annihilator, 2,7-di-tert-butylpyrene (DBP) in toluene, which is a favorable nonpolar solvent for screening TTA-UC. The UC properties of the ppy3/DBP system were also measured to serve as a reference. All three iridium complexes displayed similar absorption ranges and emission profiles with slightly red-shifted emission peaks from ppy3 to ppy2 to tmd, suggesting that ppy2 and tmd should also possess energetically favorable properties for blue-to-UV UC (**Fig. 1B**). **Fig. 1C** presents the normalized UC photoluminescence (UCPL) of the three sensitizers. Each sensitizer is paired with DBP in toluene under 447 nm excitation with varying power densities. The sensitizer concentrations in this experiment were optimized to maximize UCPL (**Table S2**), and the DBP concentration was held constant between the three systems to maintain consistency and to minimize self-absorption effects from DBP. All UCPL spectra had identical shapes when compared to photoluminescence of DBP (335 nm excitation, **Fig. 1B**). The spectral shape of the UC emission remained consistent across excitation power densities. We quantified the UC quantum yield (Φ_{UC}) (**Equation 1**) of these systems as:[60]

$$\Phi_{UC}\,(\%) = \frac{\text{Number of upconverted photons}}{\text{Number of absorbed photons}} \times 100 \qquad (1)$$

Since TTA-UC efficiency is inherently limited by the requirement to absorb two photons to emit one photon, the maximum achievable Φ_{UC} is 50%. Φ_{UC} of ppy3, ppy2, and tmd are 1.4%, 2.0%, and 3.2%, respectively (**Fig. 1D**), indicating the ppy2/DBP and tmd/DBP systems had higher UC efficiencies than the ppy3/DBP system. Another important TTA-UC metric is the threshold (I_{th}), or the power density of incident light at which UC intensity transitions from a quadratic regime (inefficient TTA) to a linear regime (efficient TTA).[61] I_{th} for the ppy3/DBP, ppy2/DBP, and tmd/DBP systems were 156, 51.5, and 115 mW/cm^2, respectively (**Fig. 1E**), which means the ppy2/DBP and tmd/DBP systems exhibited lower thresholds to achieve efficient UC than the ppy3/DBP system. In summary, using either ppy2 or tmd as a sensitizer with DBP reduced the threshold values and increased UC quantum yields compared to using ppy3 as a sensitizer.

Moving beyond bulk solutions, we found that encapsulation significantly increased upconverted light output when using either ppy2 or tmd as sensitizers. ppy3, ppy2, and tmd were encapsulated with DBP into micelles to compare UC performance of micelles to TCB solutions. Although toluene is generally a better solvent for solution upconversion due to its low polarity (**Fig. 1**),[33,45]

we switched the core solvent for micelle integration to TCB because it provides better solubility for sensitizers (**Table S1**) and facilitates the formation of more consistent and stable micelles. The encapsulation process is shown schematically in **Fig 2A**. Freshly fabricated micelles were approximately 25 nm in diameter (**Table S5**) allowing for facile dispersion in water to produce suspensions with excellent optical clarity. The spectroscopic characterization of these micelles is shown in **Fig. 2B**, with the counts of UC and phosphorescence scaled to the highest counts of ppy3/DBP micelle UC. The concentrations of materials used for micelle integration were re-optimized for each system to maximize emitted light: the TTA-UC material concentrations required for efficient micelle fabrication were consistently higher than the optimal concentrations in toluene (**Table S2**), indicating the importance of high solubility of the UC materials. More efficient upconverting micelles were produced by ppy2/DBP and tmd/DBP systems instead of ppy3/DBP because ppy2/DBP and tmd/DBP have higher intrinsic UC efficiencies (**Fig. 1D**) and higher solubilities in the TCB solvent used for micelle integration (**Fig. S1**). When adding the same total quantity of UC materials, the magnitude of UCPL is lower from TCB solution than from micelles (**Fig. 2B**). Additionally, encapsulation reduced sensitizer phosphorescence (**Fig. 2B**) and increased the UC-to-phosphorescence ratio by an order of magnitude (**Table S3**). This enhanced performance implies fewer losses from the encapsulated UC system compared to UC in TCB solution. Dramatically reduced phosphorescence has been observed in other nanoencapsulated UC systems,[29] suggesting the generalizability of these findings. However, we note that for blue-to-UV upconversion, phosphorescence is still a significant energetic loss pathway as shown in **Fig. S2**. The performance of the three UV-emitting UC micelles is summarized in **Fig. 2C**, where ppy2/DBP micelles produced the highest UC emissions and tmd/DBP micelles generated the highest UC-to-phosphorescence ratio.

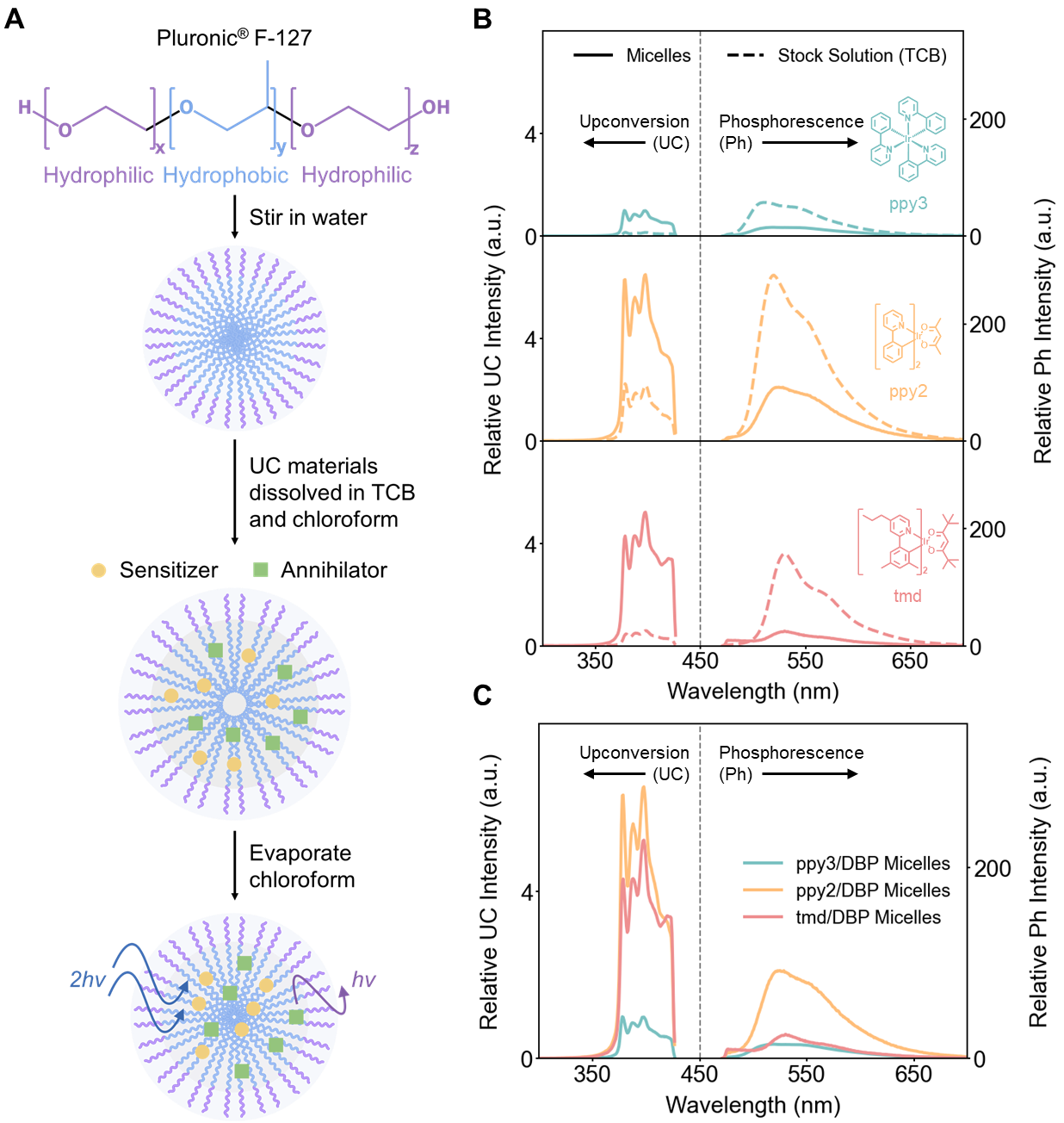

Figure 2. Nanoencapsulation of iridium complexes with DBP to form UV-emitting UC micelles. A. A schematic of the encapsulation process using F-127 micelles. **B.** Upconversion (UC) and phosphorescence (Ph) of sensitizers in both micelles and solutions (1,2,4-trichlorobenzene (TCB)) under 447 nm excitation. Constant concentrations of UC materials were used to compare TTA-UC in TCB solutions as compared to micelles (i.e., the same total quantity of UC materials was used and diluted to a constant volume). A 425 nm short pass filter was used when collecting UC emission, and a 475 nm long pass filter was used when collecting sensitizer phosphorescence.

The gray dashed line separates UC and phosphorescence. The counts of UC and phosphorescence were scaled to the highest count of ppy3/DBP micelle UC (set to 1.0). **C.** A comparison of UC and phosphorescence intensities of the three UV-emitting micelles. The concentrations used for data presented in panels **B** and **C** are summarized in **Table S2**.

Deployment into diverse applications involves different requirements such as specific UV emission ranges, elimination of metal sensitizer complexes to promote biocompatibility, or reduced costs for scalable production. Towards this end, we find an enormous flexibility to "mix and match" sensitizers and annihilators that generate UV UC emission. To assess the generalizability of the encapsulation method, five sensitizers and four annihilators—twenty distinct UC pairs—were integrated into micelles (**Fig. 3**). In addition to the aforementioned iridium complexes, we selected two pure organic sensitizers, 3,3'-carbonylbis(7-diethylaminocoumarin) (CBDAC)[43] and 2,4,5,6-tetra(carbazol-9-yl)benzene-1,3-dicarbonitrile (4CzIPN),[36] to investigate the scope of materials compatible with this encapsulation method. We encapsulated annihilators with different UV emission ranges: pyrene,[41] 1,4-bis((triisopropylsilyl)ethynyl)naphthalene (TIPS-Nph),[39,43] and 2,5-Diphenyloxazole (PPO).[40] We note that PPO emits photons at wavelengths shorter than 350 nm, which is a particularly attractive range for photochemical reactions. UC emissions from all 20 encapsulated UC systems are shown in **Fig. 3,** with each spectrum normalized to its emission at 425 nm. We found that all but one of the systems formed successful UV-emitting UC micelles. The only unsuccessful combination of CBDAC and PPO did not show UCPL in the micelle precursor TCB solution nor in toluene. Slightly red-shifted UC emissions were observed from pyrene and TIPS-Nph and are attributed to molecular aggregation.[41,43] Overall, this incredible flexibility to mix-and-match sensitizers and annihilators in micelles presents opportunities to meet the diverse requirements of a wide range of applications.

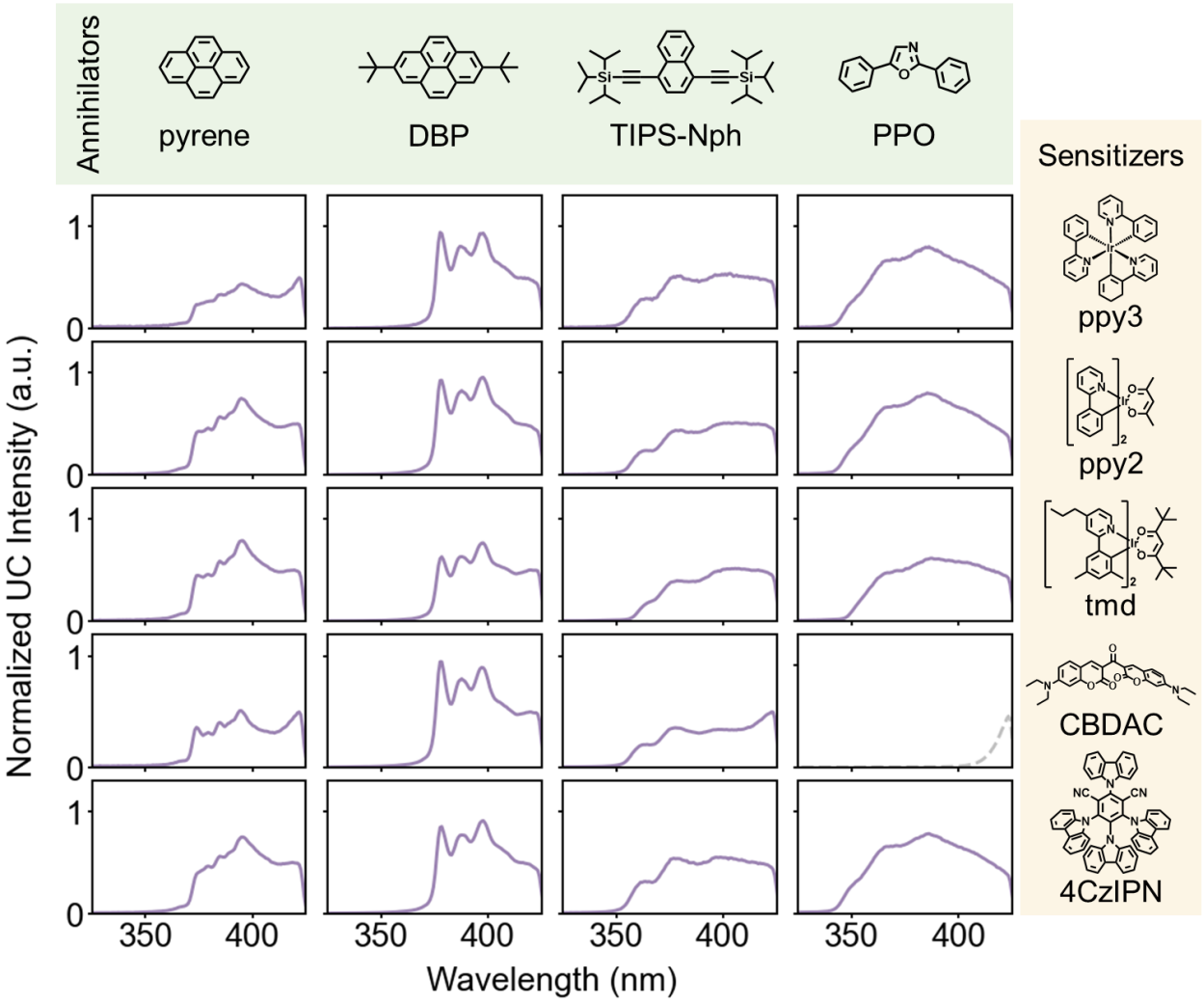

Figure 3. Mix-and-match sensitizer/annihilator pairings for blue-to-UV UC micelles. UCPL of various annihilator (each column) and sensitizer (each row) pairings under 447 nm laser excitation. The UCPL was collected through a 425 nm short pass filter. UC intensities were normalized to each spectrum emission counts at 425 nm (set to be 0.5). The concentrations used for data presented in this figure are summarized in **Table S4**.

Next, we demonstrated the utility of an encapsulated blue-to-UV system to trigger a UV-sensitive photochemical reaction in aqueous solution. Specifically, we selected a caged fluorophore with a photocleavable protecting group as a UV upconversion reporter, such that removal of the protecting group using UV photolysis results in visible color changes and measurable absorbance

and fluorescence changes. The UV upconversion reporter was fluorescein bis-(5-carboxymethoxy-2-nitrobenzyl) ether, hereafter referred to as caged fluorescein (**Fig. 4A**).[62] We hypothesized that blue incident light would photolyze caged fluorescein only when UV upconversion micelles were integrated into the solution (**Fig. 4B**). For this demonstration, we selected the ppy2/PPO sensitizer/annihilator pair due to its upconversion emission profile extending deepest into the UV spectrum (**Fig. 3**), where caged fluorescein has high absorptivity. The fabrication of ppy2/PPO micelles was optimized to maximize upconversion counts (**Fig. S3 and SI Methods**).

In a control experiment, solutions of caged fluorescein were irradiated with a 365 nm LED, which led to photolysis of caged fluorescein and visible changes from transparent to yellow (**Fig. 4C**, top row). An absorbance peak near 490 nm emerged and grew with increased UV irradiation, indicating increased concentrations of uncaged fluorescein (**Fig. 4D**). The absorbance spectrum was consistent with the spectrum of fluorescein, the uncaged product. Samples containing caged fluorescein and ppy2-only micelles (non-upconverting) did not change color (**Fig. 4C**, middle row) or absorbance (**Fig. 4E**) when irradiated with a 470 nm LED, suggesting that blue light was insufficient to photolyze caged fluorescein in the absence of a complete upconversion system. In contrast, samples containing caged fluorescein and ppy2/PPO upconversion micelles progressively changed to yellow (**Fig. 4C**, bottom row) and developed an absorbance peak near 490 nm (**Fig. 4F**) with continued exposure to a 470 nm LED. Fluorescence emission spectra showed that both UV light and blue light with ppy2/PPO upconversion micelles photolyzed caged fluorescein, with longer light exposure times corresponding to greater fluorescence intensity (**Fig. S4**). Direct irradiation with UV light photolyzed caged fluorescein more quickly than irradiation with blue light with ppy2/PPO upconversion micelles, even when the photon flux of blue incident light exceeded that of UV incident light (**Fig. 4C**, top and bottom rows, respectively). This difference in photolyzing kinetics between direct UV irradiation and upconversion micelles is attributed to relatively low UC quantum yields **(Fig. 1D**). Yet, this attribute can still be potentially advantageous in some contexts. Low UC quantum yields provide larger dynamic ranges available to control photolysis kinetics by adjusting micelle concentration and input power. The potentially large dynamic range of UC photon flux is favorable for applications such as spatiotemporal control over drug delivery, in which a high flux of UV light can be damaging to surrounding cells.[13,14]

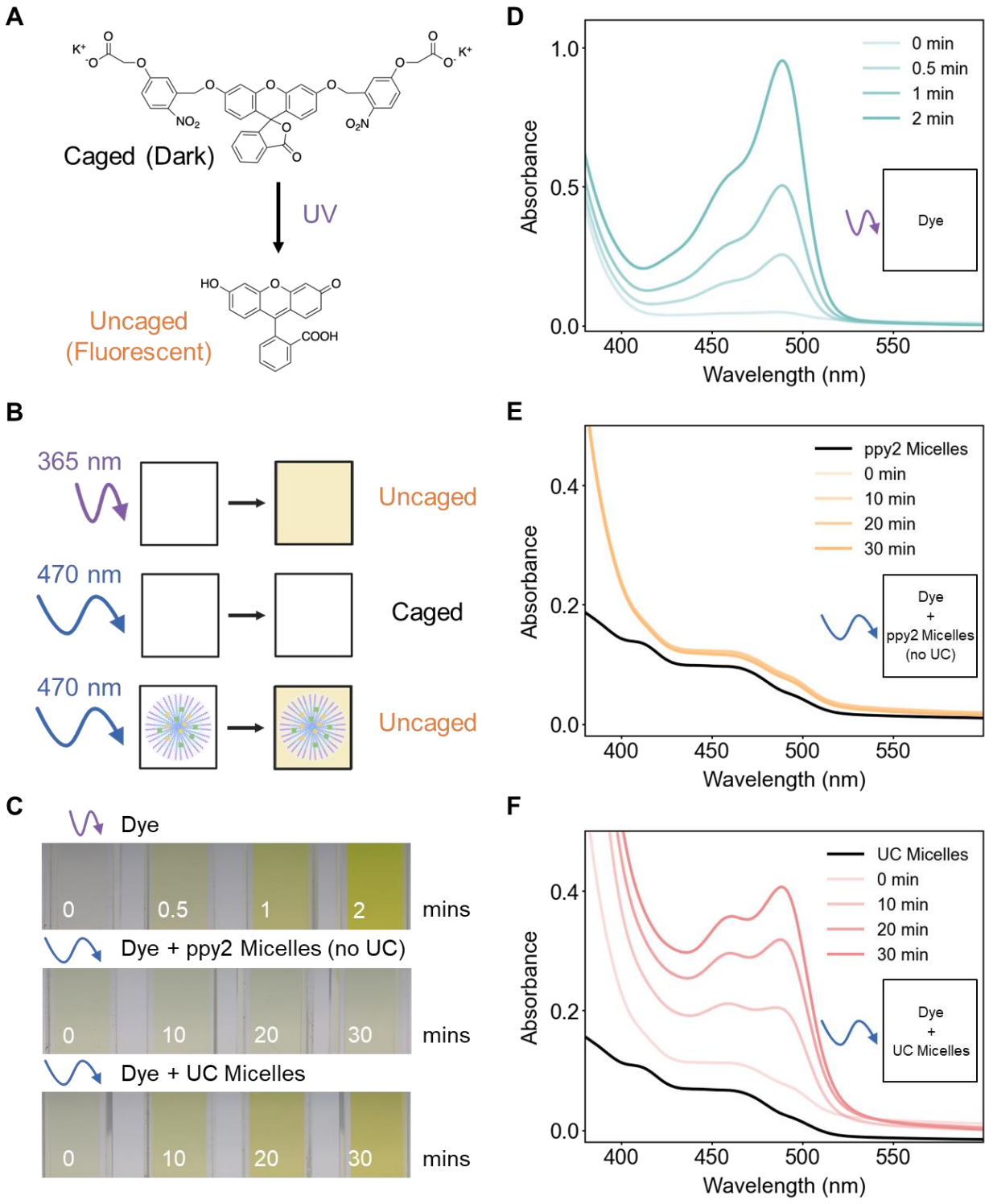

Figure 4. Blue incident light performs UV photochemistry with ppy2/PPO micelles as demonstrated by photolysis of caged fluorescein. A. Ortho-nitrobenzyl caged fluorescein is non-fluorescent until UV-triggered photolysis, which produces the uncaged product fluorescein. **B.**

Schematic demonstrating that caged fluorescein undergoes photolysis upon exposure to a 365 nm LED and displays visible color changes (top), whereas caged fluorescein does not photolyze upon exposure to 470 nm LED (middle). Incorporating ppy2/PPO upconversion micelles into a caged fluorescein solution causes fluorescein photolysis upon exposure to a 470 nm LED and subsequent blue-to-UV upconversion (bottom). **C.** 365 nm UV light (19.7 mW) photolyzed caged fluorescein in solution (top). 470 nm blue light (50.4 mW) did not photolyze caged fluorescence over a 30-minute interval (middle), but 470 nm blue light successfully photolyzed caged fluorescein when ppy2/PPO upconversion micelles were incorporated in solution (bottom). All cuvettes contained 2.5 mL of 0.2 mM caged fluorescein in 1× phosphate-buffered saline (PBS). **D, E, F.** UV-vis absorption spectra corresponding to the top, middle, and bottom rows of cuvettes shown in 4C, respectively. A characteristic fluorescein absorbance peak near 490 nm is evident after photolysis of caged fluorescein with UV light (D) or blue-to-UV upconversion (F).

Finally, we demonstrate the command of in-depth and spatially confined UV light generation using blue-to-UV UC micelles. Blue-to-UV upconversion is a powerful method for triggering UV photochemistry in scenarios that require greater incident light penetration depths than direct irradiation with UV light can achieve (**Fig. 5A**). A 365 nm LED beam was visualized with fluorescence triggered by the beam (**Fig. S5**) and noticeably attenuated across a 1 cm cuvette containing a solution of caged fluorescein (**Fig. 5B**, top). In contrast, a 470 nm LED beam did not attenuate as severely through a 1 cm cuvette containing a solution of caged fluorescein and ppy2/PPO upconversion micelles (**Fig. 5B**, bottom). The visualized 470 nm LED beam was a combination of the beam itself, sensitizer fluorescence, and upconverted UV emission. While the UV light intensity reduced by 50% after penetrating 3 mm deep into the solution, the blue light intensity decreased by less than 5% (**Fig. S6**). Surprisingly, the presence of absorptive sensitizer molecules did not significantly impact the transmission of a 470 nm beam through the cuvette containing ppy2/PPO upconversion micelles. An apparent benefit of encapsulating upconversion materials is that the overall concentration of absorptive compounds in the path of incident light is minimized, while sufficient concentrations are maintained locally in the micelle core to facilitate upconversion. These images demonstrate the potential for blue-to-UV upconversion to trigger UV photochemistry deeper within media than direct UV excitation.

UV photochemistry was further demonstrated in localized volume elements by leveraging the quadratic nature of blue-to-UV TTA-UC. Since upconversion only proceeds efficiently at regions of high intensity, the photolysis of caged fluorescein was localized to the focal point of blue input light in a system with blue-to-UV upconversion micelles (**Fig. 5C**). Focused UV light photolyzed the caged fluorescein primarily where the beam entered the solution (**Fig. 5D**, top row), and background-subtracted images revealed minimal photolysis at the focal point (**Fig. 5E**, top row). In contrast, focused blue light enabled photolysis primarily at the focal point in a solution containing ppy2/PPO micelles (**Fig. 5D**, bottom row), which became more apparent after background subtraction (**Fig. 5E**, bottom row). In summary, encapsulated blue-to-UV upconversion systems offer exquisite control over the volume and location of UV-triggered photochemical reactions. This technology enables opportunities for the precise photochemical manipulation of light-responsive materials[29,63] that are currently inaccessible with direct excitation. Looking forward, we seek to increase the spatial resolution of the UC emission by combining chemical and optical means of control.

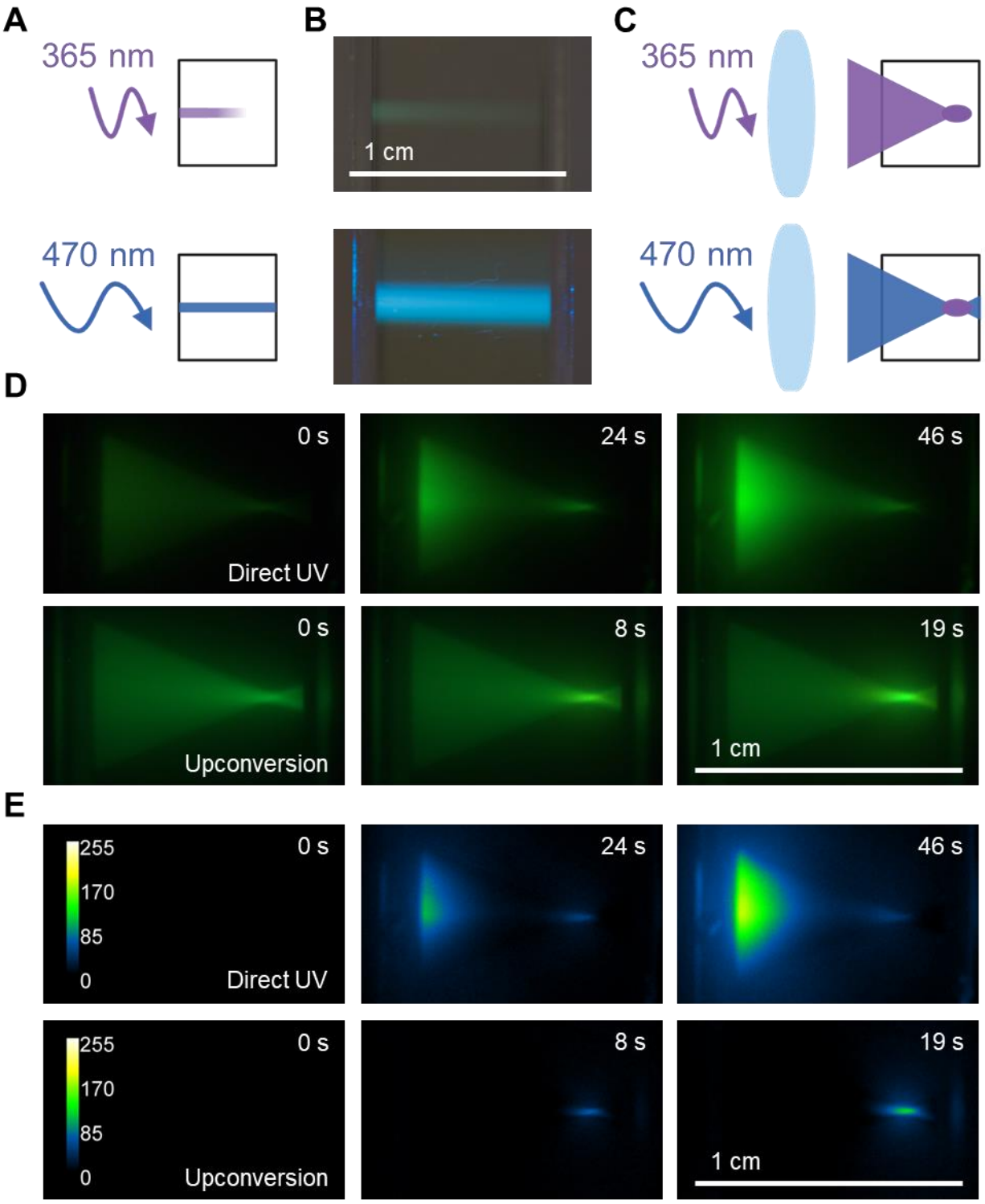

Figure 5. UC micelles enhance the penetration depth and spatial confinement of UV radiation to perform localized UV photochemistry. A. Schematic of the experimental setup for B: light beam penetration through cuvettes. **B.** UV light (365 nm) attenuates more substantially

across a 1 cm cuvette than blue light (470 nm). Both samples contain 0.2 mM caged fluorescein in 1× PBS, and the sample irradiated by blue light also contained ppy2/PPO upconversion micelles. The UV beam is visualized by fluorescence, whereas the blue beam is visualized by fluorescence, sensitizer luminescence, and annihilator upconversion emissions. Both LED sources were operated at 32 mW. **C.** Schematic of the experimental setup for C: light focused with a 50× 0.55 numerical aperture (NA) objective. **D.** Photographic images of focused UV light photolysis of caged fluorescein throughout the light path, whereas blue-to-UV upconversion confines photolysis to a voxel deep within the solution. The UV beam is visualized by fluorescence, and the blue beam is visualized by fluorescence, sensitizer luminescence, and annihilator upconversion emissions. To demonstrate photolysis, a fluorescein solution (top) and fluorescein and ppy2/PPO micelles solution (bottom) were irradiated with the same power (2.2 mW) of 365 nm UV LED and 470 nm blue LED, respectively. All cuvettes contained 1.5 mL of 0.67 mM caged fluorescein. The light was focused by a 50× 0.55 NA objective. The scientific camera was equipped with a 500 nm long pass filter. **E.** False-colored maps of fluorescein luminescence intensities after background subtraction (the intensity at t = 0 s was treated as background) illustrate that photolysis deep within a solution is enabled by an encapsulated blue-to-UV UC system.

In conclusion, we demonstrate a generalized approach to encapsulate blue-to-UV upconversion systems, which were deployed to conduct spatially controlled photochemical reactions in aqueous environments at depth. Specifically, two iridium complexes with excellent solubilities in organic solvents (e.g., toluene and TCB) were identified as sensitizers for blue-to-UV UC. The TTA-UC efficiencies of sensitizers ppy2 and tmd paired with the annihilator DBP in toluene led to both higher UC quantum yields and lower thresholds than a previously reported system, ppy3/DBP. The increased solubility of ppy2 and tmd in TCB enabled encapsulation of more molecules into Pluronic F-127 micelles, resulting in micelles with improved UC light output and reduced phosphorescence compared to unencapsulated UC pairs in organic solvents. To demonstrate the generalizability of the encapsulation method for UV-emitting TTA-UC systems, nineteen different UV UC pairs were successfully integrated into Pluronic F-127 micelles, allowing customizability in excitation wavelengths and UV emission ranges to satisfy the requirements of versatile applications. As a proof of concept, we used ppy2/PPO micelles to trigger photolysis of caged

fluorescein with upconverted UV light at a focal point deep within an aqueous solution. UV-emitting micelles provide the unique advantage of enhanced penetration depth and spatially confined light generation with low incident powers, which are inaccessible with direct excitation due to absorption and scattering effects. Precise, localized UV light generation at depth with TTA-UC has the potential to revolutionize a myriad of burgeoning fields, such as volumetric 3D printing, spatially controlled drug delivery, and precise optogenetic activation.

Acknowledgements

This work was supported by the Precourt Institute at Stanford University (Precourt Pioneering Project), the Gordon and Betty Moore Foundation, and the Departments of Chemical Engineering and Electrical Engineering at Stanford University. T.H.S. and M.C.B. gratefully acknowledge support from the Arnold and Mabel Beckman Foundation. T.H.S. was supported by the Gordon and Betty Moore Foundation. P.N. acknowledges the support of the Stanford Graduate Fellowship in Science and Engineering as a Gabilan Fellow. A.O.G. acknowledges the support of a National Science Foundation Graduate Research Fellowship under Grant DGE1656518 and a Stanford Graduate Fellowship in Science & Engineering (SGF) as a Scott A. and Geraldine D. Macomber Fellow. C.L. was supported by Stanford's Electrical Engineering summer research experiences for undergraduates (REU) program. Part of this work was performed at the Stanford Nano Shared Facilities (SNSF), supported by the National Science Foundation under award ECCS-2026822. The schematic images in Fig. 2A, 4B, 5A and 5C are created with BioRender.com.

Conflict of Interest

D.N.C. is a co-founder of and Chief Scientific Advisor to Quadratic 3D, Inc. Stanford University has filed a patent based on this work.

Contributions

Q.Z. and B.M.W. designed and performed experiments, analyzed data, and wrote the manuscript. T.H.S. and M.C.B. contributed to experimental design, data analysis, and manuscript editing. M.H., P.N., and A.O.G. helped with characterization and construction of optical setups. J.L. assisted with micelle fabrication and optimization. C.L., T.H.S., and Q.Z. worked on theoretical calculations in this manuscript. T.H.S., D.J.M., and D.N.C. supervised the research. All authors contributed to the manuscript.

References

1. Corson, E. R. *et al.* Reduction of carbon dioxide at a plasmonically active copper-silver cathode. *Chemical Communications* **56**, 9970–9973 (2020).
2. Ahmad, K., Ghatak, H. R. & Ahuja, S. M. A review on photocatalytic remediation of environmental pollutants and H2 production through water splitting: A sustainable approach. *Environmental Technology and Innovation* vol. 19 Preprint at https://doi.org/10.1016/j.eti.2020.100893 (2020).
3. Al-Mamun, M. R., Kader, S., Islam, M. S. & Khan, M. Z. H. Photocatalytic activity improvement and application of UV-TiO2 photocatalysis in textile wastewater treatment: A review. *Journal of Environmental Chemical Engineering* vol. 7 Preprint at https://doi.org/10.1016/j.jece.2019.103248 (2019).
4. Bagheri, A. & Jin, J. Photopolymerization in 3D Printing. *ACS Applied Polymer Materials* vol. 1 593–611 Preprint at https://doi.org/10.1021/acsapm.8b00165 (2019).
5. Ma, S. J., Wagner, N. J. & Kloxin, C. J. Rapid and controlled photo-induced thiol-ene wrinkle formation: Via flowcoating. *Mater Horiz* **5**, 514–520 (2018).
6. Ruskowitz, E. R. & Deforest, C. A. Photoresponsive biomaterials for targeted drug delivery and 4D cell culture. *Nature Reviews Materials* vol. 3 Preprint at https://doi.org/10.1038/natrevmats.2017.87 (2018).
7. DeForest, C. A. & Anseth, K. S. Cytocompatible click-based hydrogels with dynamically tunable properties through orthogonal photoconjugation and photocleavage reactions. *Nat Chem* **3**, 925–931 (2011).
8. Levalley, P. J. *et al.* On-Demand and Tunable Dual Wavelength Release of Antibodies Using Light-Responsive Hydrogels. *ACS Appl Bio Mater* **3**, 6944–6958 (2020).
9. Swinehart, D. F. The beer-lambert law. *J Chem Educ* **39**, 333 (1962).
10. Young, A. T. Rayleigh scattering. *Phys. Today* **35**, 42–48 (1982).
11. Andrady, A. L., Hamid, S. H., Hu, X. & Torikai, A. Effects of increased solar ultraviolet radiation on materials. *J Photochem Photobiol B* **46**, 96–103 (1998).
12. Lu, T., Solis-Ramos, E., Yi, Y. & Kumosa, M. UV degradation model for polymers and polymer matrix composites. *Polym Degrad Stab* **154**, 203–210 (2018).
13. Moan, J. & Peak, M. J. Effects of UV radiation on cells. *J Photochem Photobiol B* **4**, 21–34 (1989).
14. Karran, P. & Brem, R. Protein oxidation, UVA and human DNA repair. *DNA Repair (Amst)* **44**, 178–185 (2016).
15. Strangman, G., Boas, D. A. & Sutton, J. P. Non-invasive neuroimaging using near-infrared light. *Biol Psychiatry* **52**, 679–693 (2002).
16. Hong, G., Antaris, A. L. & Dai, H. Near-infrared fluorophores for biomedical imaging. *Nature Biomedical Engineering 2017 1:1* **1**, 1–22 (2017).
17. Franken, P. A., Hill, A. E., Peters, C. W. & Weinreich, G. Generation of Optical Harmonics. *Phys Rev Lett* **7**, 118 (1961).

18. Zhou, J., Liu, Q., Feng, W., Sun, Y. & Li, F. Upconversion luminescent materials: Advances and applications. *Chem Rev* **115**, 395–465 (2015).
19. Auzel, F. Upconversion and Anti-Stokes Processes with f and d Ions in Solids. *Chem Rev* **104**, 139–173 (2004).
20. Singh-Rachford, T. N. & Castellano, F. N. Photon upconversion based on sensitized triplet–triplet annihilation. *Coord Chem Rev* **254**, 2560–2573 (2010).
21. Weingarten, D. H. *et al.* Experimental demonstration of photon upconversion via cooperative energy pooling. *Nature Communications 2017 8:1* **8**, 1–7 (2017).
22. Pawlicki, M., Collins, H. A., Denning, R. G. & Anderson, H. L. Two-Photon Absorption and the Design of Two-Photon Dyes. *Angewandte Chemie International Edition* **48**, 3244–3266 (2009).
23. Izawa, S. & Hiramoto, M. Efficient solid-state photon upconversion enabled by triplet formation at an organic semiconductor interface. *Nature Photonics 2021 15:12* **15**, 895–900 (2021).
24. Boyd, R. W. The Nonlinear Optical Susceptibility. *Nonlinear Optics* 1–67 (2008) doi:10.1016/B978-0-12-369470-6.00001-0.
25. Grupp, A., Budweg, A., Fischer, M. P., Manzoni, C. & Cerullo, G. Design criteria for ultrafast optical parametric amplifiers. *Journal of Optics* **18**, 103501 (2016).
26. Seo, S. E. *et al.* Recent advances in materials for and applications of triplet–triplet annihilation-based upconversion. *J Mater Chem C Mater* **10**, 4483–4496 (2022).
27. Zhao, J., Ji, S. & Guo, H. Triplet–triplet annihilation based upconversion: from triplet sensitizers and triplet acceptors to upconversion quantum yields. *RSC Adv* **1**, 937–950 (2011).
28. Bharmoria, P., Bildirir, H. & Moth-Poulsen, K. Triplet–triplet annihilation based near infrared to visible molecular photon upconversion. *Chem Soc Rev* **49**, 6529–6554 (2020).
29. Sanders, S. N. *et al.* Triplet fusion upconversion nanocapsules for volumetric 3D printing. *Nature 2022 604:7906* **604**, 474–478 (2022).
30. Limberg, D. K., Kang, J. H. & Hayward, R. C. Triplet-Triplet Annihilation Photopolymerization for High-Resolution 3D Printing. *J Am Chem Soc* **144**, 5226–5232 (2022).
31. Wang, Z. *et al.* Spatially confined photoexcitation with triplet–triplet annihilation upconversion. *Chemical Communications* **57**, 9044–9047 (2021).
32. Wang, Z., Zhang, Y., Su, Y., Zhang, C. & Wang, C. Three-dimensional direct-writing via photopolymerization based on triplet—triplet annihilation. *Science China Chemistry 2022* 1–7 (2022) doi:10.1007/S11426-022-1380-6.
33. Zähringer, T. J. B., Bertrams, M. S. & Kerzig, C. Purely organic Vis-to-UV upconversion with an excited annihilator singlet beyond 4 eV. *J Mater Chem C Mater* **10**, 4568–4573 (2022).
34. Olesund, A. *et al.* Approaching the Spin-Statistical Limit in Visible-to-Ultraviolet Photon Upconversion. *J Am Chem Soc* **144**, 3706–3716 (2022).

35. Duan, P., Yanai, N. & Kimizuka, N. A bis-cyclometalated iridium complex as a benchmark sensitizer for efficient visible-to-UV photon upconversion. *Chemical Communications* **50**, 13111–13113 (2014).
36. Chen, Q. *et al.* Energy Transfer Dynamics in Triplet-Triplet Annihilation Upconversion Using a Bichromophoric Heavy-Atom-Free Sensitizer. *Journal of Physical Chemistry A* **122**, 6673–6682 (2018).
37. Gray, V. *et al.* CdS/ZnS core–shell nanocrystal photosensitizers for visible to UV upconversion. *Chem Sci* **8**, 5488–5496 (2017).
38. Okumura, K., Yanai, N. & Kimizuka, N. Visible-to-UV Photon Upconversion Sensitized by Lead Halide Perovskite Nanocrystals. *https://doi.org/10.1246/cl.190473* **48**, 1347–1350 (2019).
39. Harada, N., Sasaki, Y., Hosoyamada, M., Kimizuka, N. & Yanai, N. Discovery of Key TIPS-Naphthalene for Efficient Visible-to-UV Photon Upconversion under Sunlight and Room Light**. *Angewandte Chemie International Edition* **60**, 142–147 (2021).
40. Singh-Rachford, T. N. & Castellano, F. N. Low power visible-to-UV upconversion. *Journal of Physical Chemistry A* **113**, 5912–5917 (2009).
41. Zhao, W. & Castellano, F. N. Upconverted emission from pyrene and Di-tert-butylpyrene using Ir(ppy) 3 as triplet sensitizer. *Journal of Physical Chemistry A* **110**, 11440–11445 (2006).
42. Lin, X. *et al.* ZnSe/ZnS Core/Shell Quantum Dots as Triplet Sensitizers toward Visible-to-Ultraviolet B Photon Upconversion. *ACS Energy Lett* **7**, 914–919 (2022).
43. Uji, M. *et al.* Heavy metal-free visible-to-UV photon upconversion with over 20% efficiency sensitized by a ketocoumarin derivative. *J Mater Chem C Mater* **10**, 4558–4562 (2022).
44. Wei, Y. *et al.* Multiple Resonance Thermally Activated Delayed Fluorescence Sensitizers Enable Green-to-Ultraviolet Photon Upconversion: Application in Photochemical Transformations. *CCS Chemistry* 1–12 (2022) doi:10.31635/CCSCHEM.022.202101507.
45. Kerzig, C. & Wenger, O. S. Sensitized triplet–triplet annihilation upconversion in water and its application to photochemical transformations. *Chem Sci* **9**, 6670–6678 (2018).
46. Pfund, B. *et al.* UV Light Generation and Challenging Photoreactions Enabled by Upconversion in Water. *J Am Chem Soc* **142**, 10468–10476 (2020).
47. el Roz, K. A. & Castellano, F. N. Photochemical upconversion in water. *Chemical Communications* **53**, 11705–11708 (2017).
48. Askes, S. H. C., Bahreman, A. & Bonnet, S. Activation of a Photodissociative Ruthenium Complex by Triplet–Triplet Annihilation Upconversion in Liposomes. *Angewandte Chemie International Edition* **53**, 1029–1033 (2014).
49. Mattiello, S. *et al.* Self-Assembled Dual Dye-Doped Nanosized Micelles for High-Contrast Up-Conversion Bioimaging. *Adv Funct Mater* **26**, 8447–8454 (2016).
50. Torchilin, V. P. PEG-based micelles as carriers of contrast agents for different imaging modalities. *Adv Drug Deliv Rev* **54**, 235–252 (2002).

51. Sanders, S. N., Gangishetty, M. K., Sfeir, M. Y. & Congreve, D. N. Photon Upconversion in Aqueous Nanodroplets. *J Am Chem Soc* **141**, 9180–9184 (2019).
52. Yang, H., Guo, S., Jin, B., Luo, Y. & Li, X. Versatile, stable, and air-tolerant triplet–triplet annihilation upconversion block copolymer micelles. *Polym Chem* **13**, 4887–4894 (2022).
53. Bodratti, A. M. & Alexandridis, P. Formulation of Poloxamers for Drug Delivery. *Journal of Functional Biomaterials 2018, Vol. 9, Page 11* **9**, 11 (2018).
54. Li, Y. Y., Li, L., Dong, H. Q., Cai, X. J. & Ren, T. bin. Pluronic F127 nanomicelles engineered with nuclear localized functionality for targeted drug delivery. *Materials Science and Engineering: C* **33**, 2698–2707 (2013).
55. Ahmad, Z., Shah, A., Siddiq, M. & Kraatz, H. B. Polymeric micelles as drug delivery vehicles. *RSC Adv* **4**, 17028–17038 (2014).
56. Kile, D. E. & Chlou, C. T. Water Solubility Enhancements of DDT and Trichlorobenzene by Some Surfactants Below and Above the Critical Micelle Concentration. *Environ. Sci. Technol* **23**, 832–838 (1989).
57. Ha, S., Sun, B. I., Inskeep, W. P. & Boyd, S. A. Sorption of Nonionic Organic Compounds in Soil-Water Systems Containing a Micelle-Forming Surfactant. *Environ. Sci. Technoi* **29**, 903–913 (1995).
58. Sanders, S. N., Gangishetty, M. K., Sfeir, M. Y. & Congreve, D. N. Photon Upconversion in Aqueous Nanodroplets. *J Am Chem Soc* **141**, 9180–9184 (2019).
59. Kalyanasundaram, K. Photochemistry in microheterogeneous systems. 388 (1987).
60. Zhou, Y., Castellano, F. N., Schmidt, T. W. & Hanson, K. On the Quantum Yield of Photon Upconversion via Triplet-Triplet Annihilation. *ACS Energy Lett* **5**, 2322–2326 (2020).
61. Monguzzi, A., Mézyk, J., Scotognella, F., Tubino, R. & Meinardi, F. Upconversion-induced fluorescence in multicomponent systems: Steady-state excitation power threshold. *Phys Rev B Condens Matter Mater Phys* **78**, 195112 (2008).
62. Kobayashi, T. *et al.* Highly activatable and rapidly releasable caged fluorescein derivatives. *J Am Chem Soc* **129**, 6696–6697 (2007).
63. Arakawa, C. K. *et al.* Multicellular Vascularized Engineered Tissues through User-Programmable Biomaterial Photodegradation. *Advanced Materials* **29**, 1703156 (2017).

Supporting Information

Materials and Methods

Chemicals

All chemicals were used as received.

Bis(2-phenylpyridine)(acetylacetonate)iridium(III), Ir(ppy)2(acac) (ppy2) and bis(2-(3,5-dimethylphenyl)-4-propylpyridine)(2,2,6,6-tetramethylheptane-3,5-diketonate)iridium(III), Ir(dmppy-pro)2tmd (tmd) were purchased from Luminescence Technology Corp.

Tris(2-phenylpyridine)iridium(III), Ir(ppy)3 (ppy3) and 2,4,5,6-tetra(carbazol-9-yl)benzene-1,3-dicarbonitrile (4CzIPN) were purchased from Ossila.

2,7-di-tert-butylpyrene (DBP) and 3,3'-carbonylbis(7-diethylaminocoumarin) (CBDAC) were purchased from Tokyo Chemical Industry (TCI).

Pyrene, 2,5-Diphenyloxazole (PPO), Pluronic® F-127, toluene (anhydrous, 99.8%), 1,2,4-trichlorobenzene (TCB) (anhydrous, >99%), and chloroform (anhydrous, >99%, stabilized) were purchased from Sigma-Aldrich.

1,4-bis((triisopropylsilyl)ethynyl)naphthalene (TIPS-Nph) was purchased from HAARES ChemTech Inc. following a standard synthetic protocol.[1]

Fluorescein bis-(5-carboxymethoxy-2-nitrobenzyl) ether, dipotassium salt (CMNB-caged fluorescein) was purchased from ThermoFisher Scientific.

Micelle fabrication

Given the sensitivity of upconversion to oxygen, all solvents used for micelle fabrication were either sparged with nitrogen on a Schlenk line (>99% N_2 purity, sparge 20 mL at a time for approximately 15 minutes) or purchased anhydrous to maintain low oxygen content. Furthermore, micelle fabrication was performed in a glovebox with <0.5 ppm O_2. First, 60 mg/mL Pluronic F-127 was dissolved in MilliQ ultrapure water (18.2 MΩ·cm) with vigorous stirring. Next, a sensitizer solution with desired concentration was prepared in 1,2,4-trichlorobenzene (TCB), while an annihilator solution was prepared in chloroform. If a saturated solution was used for micelle

fabrication, excess materials were added to the solvent, and the solution was rigorously stirred and subsequently filtered with 0.22 μm PTFE filters to produce a homogenous and saturated solution. Sensitizer solutions were used within one week of preparation, whereas annihilator solutions were immediately discarded after use due to chloroform volatility. The sensitizer and annihilator solutions were mixed with a 2:3 volume ratio, respectively, to yield an upconversion solution. For a typical small-scale fabrication, 50 μL of upconversion solution was added to 2 mL F-127 in water (60 mg/mL). Then, the solution was stirred overnight at 800 rpm without the lid to allow the chloroform to evaporate. Finally, the UC micelle solution was filtered by 0.45 μm PVDF filters, yielding a transparent solution.

This fabrication method can be adapted to different scales. However, stirring speed and stirring time should be adjusted accordingly for different scales to ensure adequate mixing and micelle formation. For example, a 20-mL solution was stirred at 1600 rpm for more than 24 h before filtering. Solutions containing micelles were characterized in quartz cuvettes with lids secured by PTFE sealant tape before removal from the glovebox, unless otherwise specified.

Photoluminescence measurements

Photoluminescence (PL) measurements were collected on a custom setup. A 447 nm laser (MDL-F-447-2W, Dragon Lasers) excited the sample, PL was collected at 90 degrees using a collection lens, and the appropriate filter was used to avoid saturating the spectrometer (425 nm short pass filter for upconversion PL; 475 nm long pass filter for phosphorescence), QE Pro (QEPRO-XR, Ocean Insight).

Threshold measurements

Threshold measurements were collected on a custom setup, where a 447 nm laser was focused on the sample, and UCPL was collected at 90 degrees by the spectrometer with a 425 nm short pass filter. The power of the laser at the focal point was measured using an optical power detector (818-SL, Newport Corporation) threaded with an OD3 attenuator if necessary, and the photocurrent was reported by a Keithley 2400 sourcemeter. The image of the laser spot was captured by a CMOS scientific camera (CS165MU, ThorLabs, Inc.) and analyzed in ImageJ to determine the spot size. Different beam intensities were achieved by attenuating the laser with neutral density filters (NEK01, ThorLabs, Inc.).

The upconversion peak was integrated and plotted against excitation intensity in a log-log plot. The resulting plot was analyzed to find the linear and quadratic regimes, and the intersection between these regimes was used to interpolate the threshold intensity.

UC quantum yield measurements

UC quantum yield measurements were collected on a custom setup where a 447 nm laser excited the sample in an integrating sphere, and the resulting emission spectrum was collected by a spectrometer. Upconversion solutions were loaded into quartz cuvettes with 2 mm path lengths. The integrating sphere was calibrated using a radiometric source (HL-3P-CAL, Ocean Insight), which emits a known power at specific wavelengths. This calibration was used to convert arbitrary counts into absolute irradiance (μW/nm). Four measurements shown below were taken for each sample to calculate the UC quantum yield, which are modified from PLQY measurements developed by de Mello.[2]

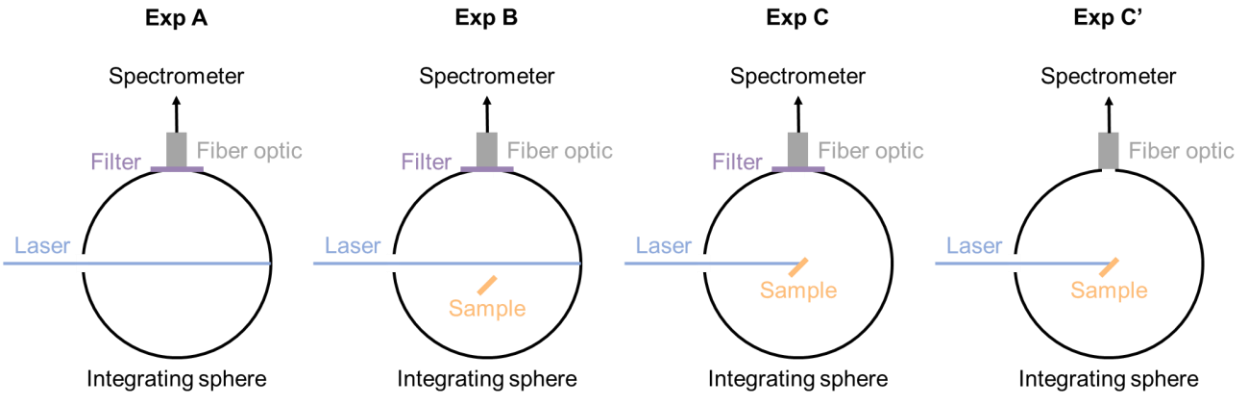

1. Exp A: There was no sample in the integrating sphere, and the emission collected from the sphere was cut off by a 425 nm short pass filter to prevent saturation of the detector.

2. Exp B: There was a sample in the integrating sphere but not in the light path, and the emission collected from the sphere was cut off by a 425 nm short pass filter to prevent saturation of the detector.

3. Exp C: There was a sample in the integrating sphere and in the light path, and the emission collected from the sphere was cut off by a 425 nm short pass filter.

4. Exp C': There was a sample in the integrating sphere and in the light path, and the emission collected from the sphere was not cut off by any filters (the detector would not saturate due to high absorption of the upconversion solution).

For each type of measurement, both UC and laser luminescence are captured by the spectrometer. The UC quantum yield was calculated as follows (*L* refers to the integrated area under the UC emission or laser profile):

$$R = \text{filter cutoff ratio on laser light} = \frac{L_{C'\_laser}}{L_{C\_laser}} \tag{2}$$

$$\text{A} = \text{absorption coefficient} = 1 - \frac{L_{C\_laser}}{L_{B\_laser}} \tag{2}$$

$$\begin{aligned} \Phi_{UC}\,(\%) &= \frac{\text{Number of upconverted photons}}{\text{Number of absorbed photons}} \times 100 \\ &= \frac{L_{C\_UC} - (1-A) \times L_{B\_UC}}{L_{A\_laser} \times A \times R} \times 100 \end{aligned} \tag{3}$$

The UC quantum yield measurement was performed once at a relatively high power density, denoted as Φ_{UC}. The power density was measured in the same way as described in the threshold measurement section. UC quantum yields (Φ'_{UC}) of other data points were calculated using the following equation by comparing their UCPL intensities and power densities with the known one:

$$\Phi'_{UC} = \Phi_{UC} \times \frac{UCPL'}{UCPL} \times \frac{power\ density}{power\ density'} \tag{4}$$

Dynamic light scattering

As-fabricated micelles were diluted 5 times with DI water and filtered with 0.22-μm PVDF filters prior to taking measurements. Samples were loaded in polystyrene cuvettes sealed with PTFE tape. A NanoBrook Omni particle size and zeta potential analyzer was used to measure micelle size distributions. Each sample was measured using three separate runs of 60 seconds each.

Other spectroscopic measurements

UV-vis absorption spectra were collected with an Agilent Cary 6000i UV/Vis/NIR. Photoluminescence data presented in **Fig. 1B** were collected with a Horiba FluoroLog Fluorimeter.

Ortho-nitrobenzyl caged fluorescein as a UV upconversion reporter

Caged fluorescein samples were prepared in a glovebox under red light conditions to prevent premature uncaging and degradation. To aid the preparation of upconversion reporter solutions, 2 mM caged fluorescein was prepared by suspending caged fluorescein powder in 1× phosphate-buffered saline (PBS) and stirring for several hours to aid dissolution. Caged fluorescein powder was stored at –20 °C between uses. Pluronic F-127 micelles were suspended in 1× PBS by adding 1 volume of 10× PBS to 9 volumes of freshly fabricated micelles in DI water.

Three distinct caged fluorescein solutions were prepared for the experiment in **Fig. 4C**:

- Positive control (**Fig. 4C**, top row): 0.2 mM caged fluorescein was produced by tenfold dilution of 2 mM caged fluorescein with nitrogen-sparged 1× PBS.
- Negative control (**Fig. 4C**, middle row): 0.2 mM caged fluorescein with sensitizer-only micelles were prepared by tenfold dilution of 2 mM caged fluorescein with nitrogen-sparged sensitizer-only micelles in 1× PBS. Sensitizer-only micelles were fabricated with saturated ppy2 in TCB and neat chloroform, in lieu of an annihilator solution.
- UC reporter (**Fig. 4C**, bottom row): 0.2 mM caged fluorescein with UC micelles were prepared by tenfold dilution of 2 mM caged fluorescein with nitrogen-sparged UC micelles in 1× PBS. UC micelles were fabricated with saturated ppy2 in TCB and 200 mM PPO in chloroform (see **Fig. S3** for concentration optimization).

From each solution, 2500 μL was distributed into four quartz cuvettes. Each cuvette was irradiated by an LED for a different amount of time. The positive control was irradiated by a 365 nm LED (ThorLabs, Inc.) at 19.7 mW. The negative control and experiment were irradiated by a 470 nm LED (ThorLabs, Inc.) at 50.4 mW. Power measurements were taken with a standard photodiode power sensor and compact power and energy meter console (S120VC and PM100D, ThorLabs, Inc.). All images were taken using a Canon EOS Rebel T6i. The reported images are unedited.

Table S1. Solubility of three iridium complexes in organic solvents at room temperature determined by UV-vis absorption spectroscopy.

Complex	Toluene (mM)	1,2,4-trichlorobenzene (TCB) (mM)
ppy3	< 0.3	< 0.7
ppy2	< 2.0	< 5.6
tmd	> 15	> 15

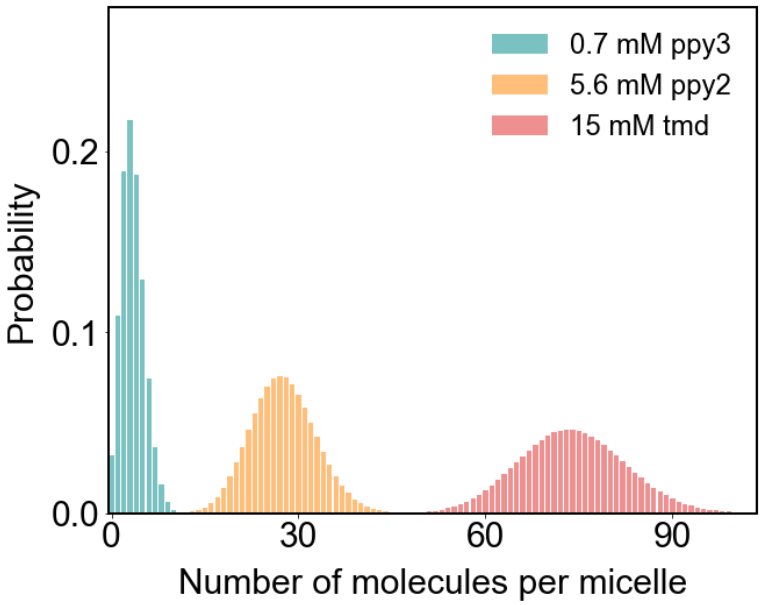

Figure S1. Theoretical prediction of the number of molecules per micelle based on concentrations in solutions added for micelle fabrication using a Poisson distribution. In this model,[3] the total number of available molecules are distributed among nanodroplets of TCB according to a Poisson probability distribution. An upper boundary of the number of nanodroplets available is determined by the TCB solution volume (20 μL) used to make micelles (for simplicity, we assume all the chloroform initially added evaporates). In this simulation, we estimate a nanodroplet diameter of 25 nm based on DLS. This is an upper boundary condition, as it is difficult to estimate the true volume of the nanodroplet in the F-127 micelle core.

Table S2. Optimized concentrations of [Sensitizer]/[Annihilator] in bulk solution (toluene) and for TCB/chloroform solutions used to prepare micelles.

Sensitizer/Annihilator pair	Solution (toluene)	Micelles (TCB/chloroform)
ppy3/DBP	[100 μM]/[1 mM]	[0.7 mM]/[50 mM]
ppy2/DBP	[200 μM]/[1 mM]	[5.6 mM]/[60 mM]
tmd/DBP	[80 μM]/[1 mM]	[15 mM]/[300 mM]

Table S3. UC-to-phosphorescence ratios of [Sensitizer]/[Annihilator] in TCB and micelles

Sensitizer/Annihilator pair	Solution ($x10^{-5}$) (TCB)	Micelles ($x10^{-5}$)
ppy3/DBP	1.3	25
ppy2/DBP	3.8	31
tmd/DBP	2.1	98

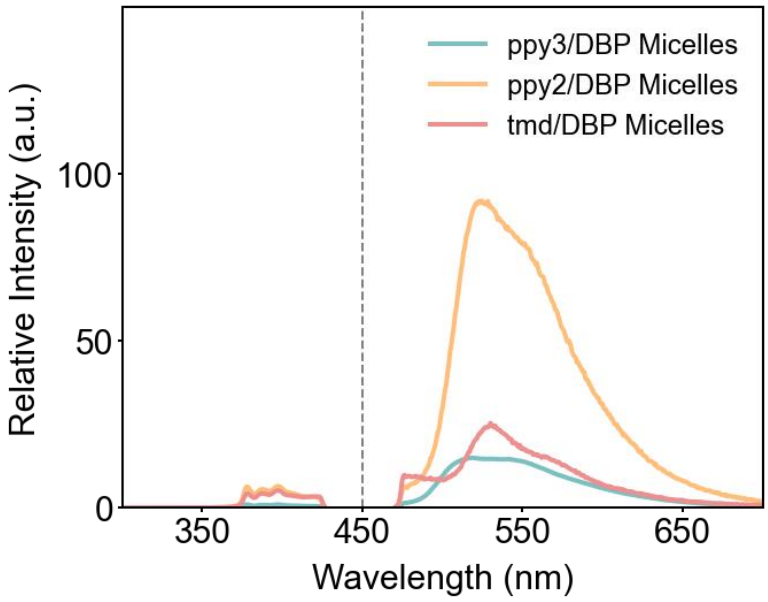

Figure S2. UV-emitting UC micelles exhibit energetic losses to phosphorescence. UC and phosphorescence intensities of three UV-emitting micelles plotted on the same y-axis scale. UC and Ph are separated by the gray dashed line. The counts of UC and Ph are scaled to the highest count of ppy3/DBP micelle UC.

Table S4. Concentrations of [Sensitizer]/[Annihilator] in TCB/chloroform solutions used to fabricate UV-emitting UC micelles in Fig. 3.

Sensitizer/ Annihilator	Pyrene	DBP	TIPS-Nph	PPO
ppy3	[0.7 mM]/[25 mM]	[0.7 mM]/[50 mM]	[0.7 mM]/[25 mM]	[0.7 mM]/[100 mM]
ppy2	[5.6 mM]/[25 mM]	[5.6 mM]/[60 mM]	[5.6 mM]/[25 mM]	[5.6 mM]/[100 mM]
tmd	[15 mM]/[25 mM]	[15 mM]/[300 mM]	[15 mM]/[125 mM]	[15 mM]/[600 mM]
CBDAC	[2 mM]/[25 mM]	[2 mM]/[50 mM]	[2 mM]/[25 mM]	[2 mM]/[100 mM]
4CzIPN	[4.3 mM]/[25 mM]	[4.3 mM]/[50 mM]	[4.3 mM]/[25 mM]	[4.3 mM]/[100 mM]

Note: Saturated TCB solutions of ppy3, ppy2, and 4CzIPN were used for fabrication, and the corresponding concentrations were determined by UV-vis absorption spectroscopy.

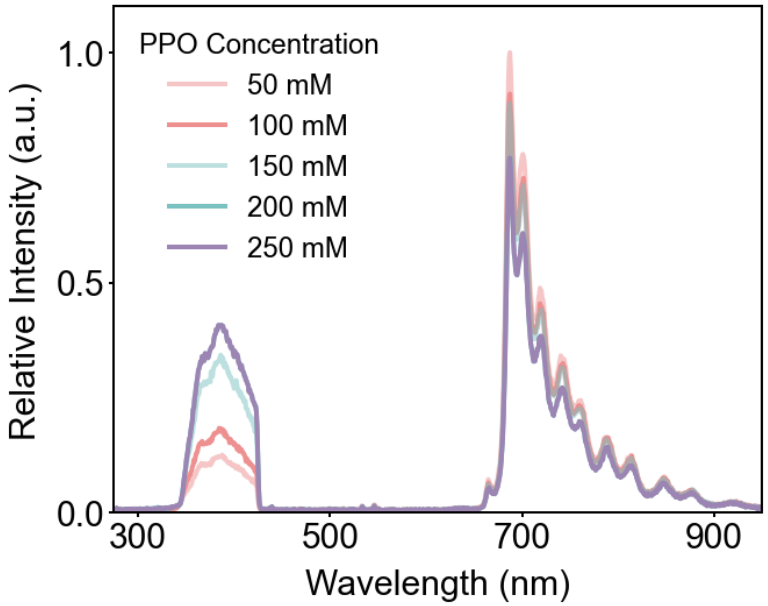

Figure S3. Optimizing upconverted PPO emission in micelles. Upconversion photoluminescence (UCPL) measurements with 447 nm laser incident light demonstrate that the maximum upconversion intensity (<425 nm) is achieved with micelles made with 200 mM PPO in chloroform. No distinguishable improvement was observed upon increasing the concentration to 250 mM, so ppy2/PPO upconversion micelles were fabricated with saturated ppy2 in TCB and 200 mM PPO in chloroform. A 425 nm short pass filter was placed in front of an Ocean Optics QE Pro detector, resulting in low intensities between 425 nm and 650 nm and influencing the spectral shape of the sensitizer luminescence above 650 nm. Each micelle UCPL spectrum was scaled by the maximum of the 50 mM spectrum to preserve relative intensity.

Table S5. Representative dynamic light scattering (DLS) data for micelles with different encapsulated species.

Micelle Contents	TCB/$CHCl_3$ only	ppy2/PPO in TCB/$CHCl_3$	ppy2 in TCB/$CHCl_3$	PPO in TCB/$CHCl_3$
Effective diameter (nm)	23.8 ± 0.2	25.6 ± 0.2	25.0 ± 0.2	24.6 ± 0.3
Polydispersity	0.12 ± 0.02	0.105 ± 0.004	0.09 ± 0.01	0.09 ± 0.02
Data retained (%)	95.2	91.8	94.8	93.3

Note: Micelles were fabricated as reported in Methods. Micelles containing ppy2 were prepared with a saturated sensitizer solution, whereas those that did not contain ppy2 were prepared with an equal volume of neat TCB. Micelles containing PPO were prepared with a 200 mM in chloroform annihilator solution, whereas those that did not contain PPO were prepared with an equal volume of neat chloroform. As-fabricated micelles were diluted by a factor of 5 with DI water and filtered with a 0.22-μm PVDF syringe filter prior to taking measurements with a NanoBrook Omni particle size and zeta potential analyzer. Values reported are the mean ± the standard deviation of three 60-second measurements.

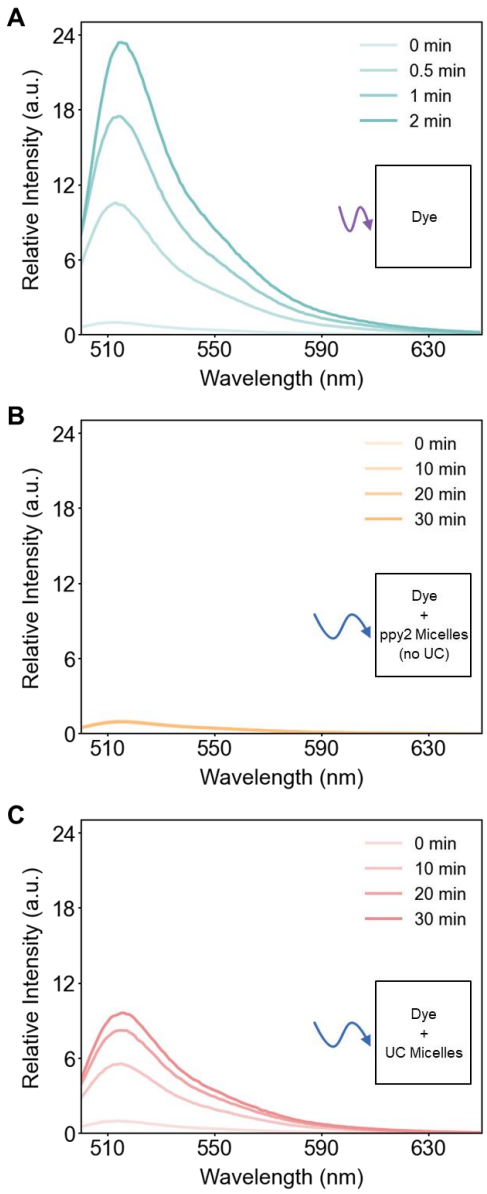

Figure S4. Fluorescence changes of caged fluorescein solutions indicate successful photolysis with incident UV light or blue light with ppy2/PPO micelles. Fluorescence data of samples presented in **Fig. 4C**. **A.** 365 nm UV light (19.7 mW) photolyzed caged fluorescein in solution, as demonstrated by a drastic increase in fluorescence. **B.** 470 nm blue light (50.4 mW) did not photolyze caged fluorescence over a 30-minute interval. **C.** 470 nm blue light (50.4 mW) photolyzed caged fluorescein when ppy2/PPO upconversion micelles were incorporated in solution. All curves on each graph are scaled by the maximum fluorescence intensity for the 0-minute cuvette to preserve relative fluorescence intensity. Emission spectra for A were taken with 470 nm excitation to prevent detector saturation, whereas B and C used 494 nm excitation.

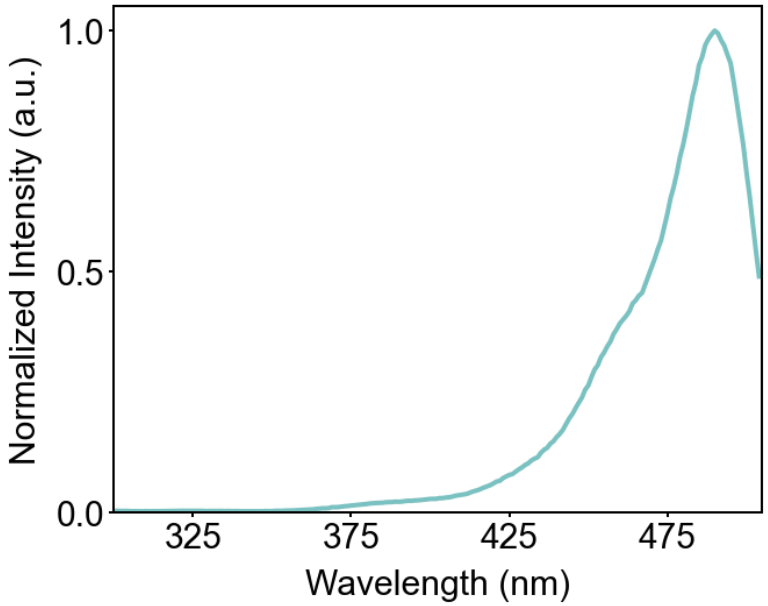

Figure S5. UV and blue light excite uncaged fluorescein. Excitation spectrum of the sample irradiated by 365 nm light for 30 s (**Fig. 4C**, top row) shows that blue and UV light excite uncaged fluorescein. Emission intensity at 512 nm was monitored, and the displayed spectrum was scaled by the maximum measured emission intensity.

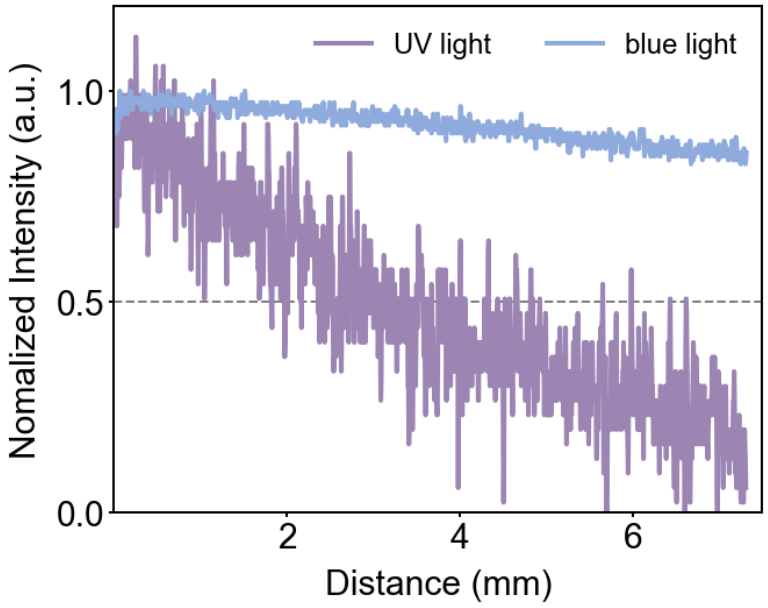

Figure S6. Normalized intensity of the incident beams across the quartz cuvettes in Fig. 5B. ImageJ was used to split images into blue, green, and red color channels. Then, gray values of the green channel were extracted to quantify the attenuation of incident beams across the quartz cuvettes.

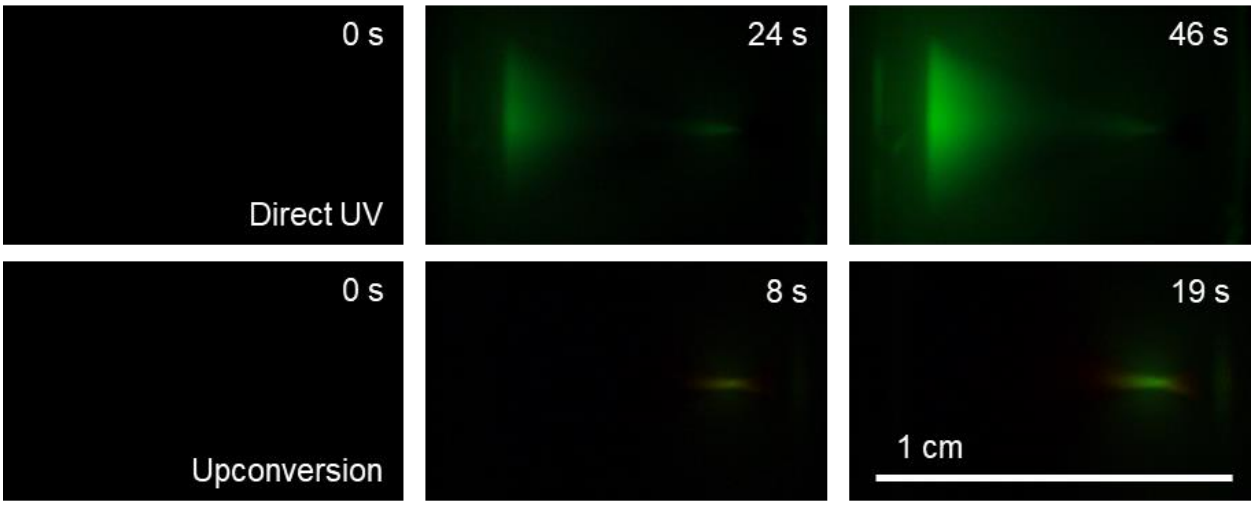

Figure S7. Localized photolysis is demonstrated by background subtracted images of fluorescein solution (top) and fluorescein and ppy2/PPO micelles solution (bottom) irradiated with the same power of 365 nm UV LED and 470 nm blue LED over time, respectively. The light was focused by a 50×, 0.55 NA objective. The camera was equipped with a 500 nm long pass filter. The images at t = 0 were used as the background for subtraction.

References

1. Harada, N., Sasaki, Y., Hosoyamada, M., Kimizuka, N. & Yanai, N. Discovery of Key TIPS-Naphthalene for Efficient Visible-to-UV Photon Upconversion under Sunlight and Room Light. *Angewandte Chemie - International Edition* **60**, 142–147 (2021).
2. de Mello, J. C., Wittmann, H. F., & Friend, R. H. An improved experimental determination of external photoluminescence quantum efficiency. *Advanced Materials* **9**, 230–232 (1997).
3. Kalyanasundaram, K. Photochemistry in microheterogeneous systems. 388 (1987).